University of Iceland
Faculty of Natural Sciences
Department of Chemistry

Theoretical Calculations of Electrochemical Systems

by

Jón Bergmann Maronsson

Thesis for the degree of
Magister Scientiarum in Chemistry
September 2008

Thesis Advisor: Professor Hannes Jónsson
Co-Advisor: Associate Professor Yoshitada Morikawa
External Examiner: Professor Viðar Guðmundsson

Hér með lýsi ég því yfir að ritgerð þessi er samin af mér og að hún hefur hvorki að hluta né í heild verið lögð fram áður til hærri prófgráðu.

Reykjavík, 29. september 2008,

Jón Bergmann Maronsson

Abstract

We present a method of manipulating electrons in a metal slab to simulate an electrochemical cell using an applied voltage in planewave DFT calculations. Periodic boundary conditions are used to simulate an infinite crystal slab. By setting the top and bottom layer of a slab at different potentials, electrons are pushed from one side to the other; creating two oppositely charged surfaces. This effect depends on the electric field that is produced in the vacuum between periodic cells. We compare this method to applying a saw tooth potential, previously used by others, and discover that our method gives a better description of the electron transfer.

We also briefly discuss the development of our method to include a potential profile similar to the electrical double layer near the metal surface. With our method we get the right features of the potential profile when electrons have been transferred to the surface, while the sow tooth potential gives exactly the opposite direction of the potential profile with regards to the electron transfer. We believe this could be a useful method when calculating adsorption energies of different species as a function of bias.

We also discuss the usage of a potential energy surface based on the single center multipole expansion in a QM/MM context with DFT calculations. This opens the possibility of using DFT calculations for the active region at the interface, while the bulk water phase is described with the less computationally demanding potential energy surface.

Ágrip

Við setjum fram aðferð til að eiga rafeindir málmfilmu með ytra mætti í DFT reikningum með planbylgjum. Lotubundin jaðarskilyrði eru notuð til að líkja eftir óendanlegum kristal. Með því að hafa efsta lag filmunnar með lægra mætti en það neðsta má þvinga rafeindir í efra lagið. Þannig myndast tveir fletir með mótstæða heðslu. Þessi rafeindafærsla er háð rafsviðinu sem myndast í tómarúminu á milli lotubundnu ímynda filmunnar. Þessi aðferð er borin saman við leggja á kerfið jafnt rafsvið, líkt og aðrir hafa gert, og í ljós kemur að okkar aðferð gefur betri lýsingu á rafeindaflutningnum.

Stuttlega verður fjallað um þróun ytra mættisins til að líkja eftir mætti tvílags nærri málmyfirborðinu. Þessi aðferð getur gefið mætti sem lítur rétt út. Til samanburðar gefur jafna rafsviðið mætti sem lítur öfugt út miðað við rafeindaflutninginn. Við höfum trú á að þetta mætti okkar geti verið mjög gagnlegt þegar ásogsorkur eru reiknaðar við mismunandi svið.

Einnig verða rædd not mættisyfirborða sem byggð eru á einmiðju fjölpóla röðinni í QM/MM samhengi við DFT reikninga. Þetta opnar á möguleika að lýsa virka svæðinu við skilin með DFT reikningum en lýsa vatninu með mættisyfirborðinu sem er ekki eins þungt í reikningum.

Acknowledgements

- Professor Hannes Jónsson, at the University of Iceland, for his guidance and inspiration.
- Associate Professor Yoshitada Morikawa, at the University of Osaka, for his guidance and kind manner while I was in a strange culture.
- Egill Skúlason for collaboration, discussions and proof-reading.
- The members of the Jónsson research group, at the University of Iceland, for enlightening discussions and support:
  - Sigríður Guðmundsdóttir, also for proof-reading
  - Jón Steinar Garðarsson Mýrdal
  - Andreas Pedersen
  - Jean-Claude Berthet, Ph.D.
  - Peter Klüpfel, Ph.D.
- The members of the Jónsson research group, at the University of Iceland, for help with compilation issues, discussions and proof-reading:
  - Andri Arnaldsson, Ph.D.
  - Finnbogi Óskarsson
- The members of the Yoshida research group, at the University of Osaka, for discussions, help and kind acceptance in a strange culture:
  - Susumu Yanagisawa, Ph.D.
  - Ikutaro Hamada, Ph.D.
  - Kunihiko Yamauchi, Ph.D.
- Friends and family for putting up with my studies for such a long time.
- Computer facilites: Bjólfur, Jötunn and Itanium
- Funding:
  - Japanese Government (MONBUKAGAKUSHO:MEXT) Scholarship
  - Science Institute of the University of Iceland

Contents

List of Figures

Chapter 1

Introduction

Electro-catalysis play a fundamental role in modern society, as they are used in batteries for various applications and in today's industry, *e.g.* in the production of aluminum, to name a few of their uses. Recently they have become quite an active research topic as plans are in the works to exchange fossil fuels for something more environmentally friendly, *e.g.* hydrogen, as an energy carrier. For that we would need to split water electrochemically to make oxygen and hydrogen, the latter of which would then be used in a fuel cell to make electricity.

A catalyst is a substance which reduces the activation energy of a given reaction and therefore changes the kinetics of that reaction. Heat and pressure are often used at the industrial scale to speed up reactions. Typically, most electro-catalytic reactions take place at ambient conditions. A solid catalyst is used as before, to reduce the activation energy, but electrons are now fed into the electrode or removed from it, to change the thermochemistry of the reaction or to make the reaction more favorable.

Modeling catalysis taking place in an electrochemical cell can be very computationally demanding. It requires the calculation of the charged metal surface, the solution with its solvated ions and the charge-transfer taking place at the solid-liquid interface during the reaction. Certain sacrifices can be made to increase the speed of the calculations. The metal can be represented by a thin film of only a few layers of crystal, the solution can be modelled using only a few molecules and so forth.

With recent advances in computing power, both with ever increasing speed and

capacity of the hardware in question and with advances in parallel computing, heavy calculations of chemical systems have become much more viable than before.

Plane-wave Density Functional Theory (DFT) calculations have aided surface science calculations greatly as entire crystals can be represented by a unit cell that is repeated to simulate an infinite crystal. Another boon of DFT calculations is their scaling, N^3, while still maintaining the accuracy of a quantum mechanical method. DFT calculations are thus quite useful in getting a better understanding of an electrochemical system and are used by many research groups around the world.

Electrochemical reactions take place at the interface between the electrode and the electrolyte. It is therefore important to understand the structure of this charged metal-liquid interface; the environment in which the reactions take place, both spatially and electrostatically.

This work discusses the solid-liquid interface in two ways. Firstly by mixing quantum mechanical calculational methods with less computationally intense calculations to better simulate the effect of bulk water near the metal surface, see chapter 3. Secondly by investigating the electrode potential profiles that are present at the metal-liquid interface, see chapter 4.

Chapter 2

Methods

2.1 Density Functional Theory

With the advances in computing power in recent years, both with more powerful computers and parallel computing, intensive calculations have become more viable. One such method is Density Functional Theory (DFT), which can be used to approximate a solution to the Scrödinger equation (section 2.1.1) for many-electron systems using *ab initio* (from the beginning) methods.

What is, perhaps, most remarkable about DFT is the fact that it is founded in *ab initio* methods and as such has not been fitted to any experimental results on chemical bonding.

The founding father of DFT is Walter Kohn who received the Nobel Prize in chemistry for his development of the density functional theory [1] in 1998 along with John Pople who received the prize for his development of computational methods in quantum chemistry [2].

2.1.1 The Schrödinger equation

A system of N electrons can be described by the Schrödinger equation,

$$\widehat{H}\Psi = E\Psi, \tag{2.1}$$

where $\Psi = \Psi(\mathbf{r}_1, \mathbf{r}_2, ..., \mathbf{r}_N)$ is the wave function, depending on the spatial coordinates, $\mathbf{r}_i$, of each electron, E is the electronic energy of the system and $\widehat{H}$ is the hamiltonian,

$$\widehat{H} = \widehat{K} + \widehat{U} + \widehat{v}, \tag{2.2}$$

with

$$\widehat{K} = \sum_i -\frac{1}{2}\nabla_i^2, \tag{2.3}$$

$$\widehat{U} = \sum_i \sum_{j>i} \frac{1}{r_{ij}}, \tag{2.4}$$

and

$$\widehat{v} = \sum_i \sum_A \frac{1}{r_{iA}} + V_{\text{ext}} \tag{2.5}$$

where $\widehat{K}$ is the kinetic part, $\widehat{U}$ is the interaction between electron pairs and $\widehat{v}$ is the interaction between electrons and the environment, called the ionic and external part. In equation 2.4 r_{ij} is the distance from electron j to electron i. In equation 2.5 the $\frac{1}{r_{iA}}$ term is the interaction between the electrons and the nucleus while V_{ext} is any other external influence.

2.1.2 The Hohenberg-Kohn Theorem

According to the Hohenberg-Kohn (H-K) theorem there is a one-to-one correspondence between the wavefunction and the electron density of the ground state. Once this has been established, it is simple to see that the total energy is a unique functional of the electron density, $\rho(\mathbf{r})$, which is an observable while the wavefunction is not,

$$E[\rho] = \langle \Psi[\rho] | \widehat{H} | \Psi[\rho] \rangle. \tag{2.6}$$

The Raleigh-Ritz variational principle is used to minimize the energy and find the ground state and density,

$$E_0 = \min_{\rho(\mathbf{r})} \left(E[\rho(\mathbf{r})] \right). \tag{2.7}$$

This is the basis of DFT, developed by Hohenberg and Kohn [3] in 1964.

2.1.3 The Kohn-Sham Equations

Currently there is no known way to perform the one-to-one mapping suggested by the H-K theorem. However in 1965 Kohn and Sham (K-S) published an indirect approach for calculating the energy functional $E[\rho]$ [4]. They showed that the interacting many-electron system can be mapped, approximately, onto a non-interacting system of single electron states, $\{\phi_i\}$, where each electron is subject to the effective potential $v_{eff}(\mathbf{r})$ due to all other particles. These one electron wavefunctions can be produced by solving the K-S equations,

$$\left\{-\frac{1}{2}\nabla^2 + v_{\text{eff}}(\mathbf{r})\right\}\phi_i(\mathbf{r}) = \epsilon_i\phi_i(\mathbf{r}). \tag{2.8}$$

Since both the effective potential and the wavefunctions are unknown these equations must be solved self-consistently. The electron density can then be produced using the square of the wavefunctions,

$$\rho(\mathbf{r}) = \sum_{i=1}^{N} |\phi_i(\mathbf{r})|^2 . \tag{2.9}$$

The effective potential can be written as

$$v_{\text{eff}}(\mathbf{r}) = v(\mathbf{r}) + v_H(\mathbf{r}) + v_{XC}(\mathbf{r}) \tag{2.10}$$

where $v(\mathbf{r})$ is the sum of the potential due to the kinetic and ionic parts in equation 2.2, $v_H(\mathbf{r})$ is the Hartree potential,

$$v_H(\mathbf{r}) = \int d^3r \frac{\rho(\mathbf{r}')}{|\mathbf{r} - \mathbf{r}|}, \tag{2.11}$$

and

$$v_{XC}(\mathbf{r}) = \frac{\delta E_{XC}[\rho]}{\delta\rho(\mathbf{r})} \tag{2.12}$$

is the potential due to the exchange-correlation functional, $E_{XC}[\rho]$, which will be discussed in section 2.1.4

2.1.4 The Exchange-Correlation Functional

The Kohn-Sham equations are in principle exact, however the exchange-correlation functional, $E_{XC}[\rho]$, is generally not known and has to be approximated. The ac-

curacy of the approximation becomes a major issue in solving the Kohn-Sham equations.

The exchange-correlation functional is a local functional which describes the electron-electron interaction,

$$E_{XC}[\rho] = \int d^3r\, \epsilon_{XC}(\rho, \mathbf{r})\rho(\mathbf{r}) \tag{2.13}$$

where $\epsilon_{XC}(\rho, \mathbf{r})$ is the exchange-correlation energy density.

The approximations used in our work are based on the so-called Generalized Gradient Approach (GGA). The GGA uses the the exchange-correlation energy of a homogeneous electron gas at point $\mathbf{r}$ like the Local Density Approximation (LDA) [4] but also uses the gradient of the density to account for inhomogeneity. This, however, is not a good choice by itself so a reduced density gradient, $s(\mathbf{r})$, is used, as suggested by Langreth and Perdew [5]. The exchange-correlation functional then becomes

$$E_{XC}^{GGA}[\rho] = \int d^3r\, \epsilon_{XC}^{GGA}(\rho(\mathbf{r}), s(\mathbf{r}))\rho(\mathbf{r}) \tag{2.14}$$

with

$$s(\mathbf{r}) = \frac{|\nabla\rho(\mathbf{r})|}{2\sqrt[3]{3\pi^2\rho(\mathbf{r})}\rho(\mathbf{r})}. \tag{2.15}$$

The calculations in chapter 3 use GGA based on the PBE functional [6] while the calculations in chapter 4 use GGA based on the RPBE functional [7].

2.1.5 The Plane Wave Basis Set

In implementing DFT calculations, the Kohn-Sham wavefunctions are expanded in a particular basis set. In our work plane waves are used under periodic boundary conditions in accordance with Bloch's theorem,

$$\psi_{\mathbf{k}}^m(\mathbf{r}) = \sum_{\mathbf{G}} c_{\mathbf{k}+\mathbf{G}}^m\, e^{i(\mathbf{k}+\mathbf{G})\cdot\mathbf{r}} \tag{2.16}$$

where $\mathbf{G}$ are the reciprocal lattice vectors. For an exact solution, an infinite number of plane waves is needed. Fortunately the plane waves at the lower end of the kinetic energy range are the most important, so the number of plane waves can be reduced by defining a cutoff, G_{cut}, where the solution becomes good

enough:

$$\left(\frac{\hbar^2}{2m}\right)|\mathbf{k}+\mathbf{G}_{cut}|^2 \leq E_{\text{cut}}. \tag{2.17}$$

This leads to one of the main advantages of plane waves. By increasing the cutoff the accuracy of the calculation can be systematically increased.

A disadvantage of plane waves is their inefficiency to deal with high curvature regions, such as the atomic core. To overcome this pseudopotentials can be used. In the core, pseudopotentials are an average of the potential due to the core electrons and the nucleus felt by the valence electrons inside a given sphere but outside the sphere the pseudopotential becomes identical to the all-electron potential. The plane-wave cutoff can be lowered even further when using pseudopotentials while generally giving results of good accuracy, especially the so-called ultrasoft pseudopotential with non-local components [8].

2.2 The Single Center Multipole Expansion

The single center multipole expansion represents a molecule as a multipole at its center of mass. Interactions between the molecules are then based on these multipoles.

In the case of water for which this expansion is used in the current work, it has been shown that in order to reach convergence in the electric field at short distances the expansion must be carried out up to and including the hexadecapole [9, 10].

2.2.1 The Multipole Expansion

The potential, at a point $\mathbf{r}$, outside a given sphere due to a charge density $\rho(\mathbf{r}')$ localized within the sphere can be written as an expansion in spherical harmonics, $Y_{lm}(\theta,\phi)$,

$$V(\mathbf{r}) = \sum_{l=0}^{\infty}\sum_{m=-l}^{l}\frac{4\pi}{2l+1}q_{lm}\frac{Y_{lm}(\theta,\phi)}{\mathbf{r}^{l+1}}. \tag{2.18}$$

To find the coefficients, q_{lm}, we look at the more common description of the charge-potential relationship,

$$V(\mathbf{r}) = \int \frac{\rho(\mathbf{r}')}{|\mathbf{r} - \mathbf{r}'|} d^3r' \tag{2.19}$$

where the integration is over all electrons in the universe. We now expand $1/|\mathbf{r}-\mathbf{r}'|$ in spherical harmonics [11]:

$$V(\mathbf{r}) = 4\pi \sum_{l=0}^{\infty} \sum_{m=-l}^{l} \frac{1}{2l+1} \left[\int Y_{lm}^*(\theta', \phi')(r')^l \rho(\mathbf{r}') d^3r' \right] \frac{Y_{lm}(\theta, \phi)}{r^{l+1}}. \tag{2.20}$$

By comparing equations 2.20 and 2.18 an expression for the coefficients, q_{lm}, in the latter can be devised:

$$q_{lm} = \int Y_{lm}^*(\theta', \phi')(r')^l \rho(\mathbf{r}') d^3r'. \tag{2.21}$$

These coefficients are called the multipole moments and can be easily calculated.

The multipole expansion can also be derived using the Taylor expansion and cartesian coordinates but it becomes much more cumbersome to write out.

2.3 Bader analysis

In our work partial charges are of particular interest. To analyze partial charges a partitioning scheme must be assumed. We utilize a scheme based on charge density, since it is readily available from the calculations, Bader's "atoms in molecules" approach [12]. Each "Bader atom" is enclosed in a zero-flux surface on which the gradient of the electron density vanishes normal to the surface. All charge within each surface is then attributed to that Bader atom.

Henkelman et al. [13] have developed an efficient algorithm for partitioning charge density using Bader's method. This algorithm lays a grid over the whole volume of the system and calculates from each grid point a steepest ascent along the direction that maximizes the charge density gradient. This is repeated until a maximum in the charge density is found. All grid points then get assigned to a charge density maximum and thereby the Bader volume associated with that maximum. If a point is found to lead to an old trajectory that point is assigned to

the same maximum as the trajectory. This way no point has to be passed twice and therefore the work needed to calculate the charge density partition scales linearly with the number of grid points.

Chapter 3

Implementing a potential energy surface in a DFT program

3.1 Introduction

Computers have improved greatly recently, both in processing power and in their ability to utilize paralellism through hardware and software development. Even with this increase in power, current computers are only able to handle a relatively small number of atoms in quantum mechanical (QM) calculations. Even DFT, which scales better than most other QM methods, N^3, is not able to handle more than 100-200 atoms in any reasonable amount of time. It is quite easy to think of a system that exceeds this limitation, *e.g.* proteins or bulk water.

To avoid this limitation different, less computationally demanding methods can be used to simulate most of the system while QM methods are used for the portion of the system where the important chemistry is happening, *e.g.* the reaction site of a protein or the surface of a metal that is submerged in water. These computationally less demanding methods can be implemented in many different ways but most are in some way based on newtonian dynamics, often referred to as molecular mechanics (MM).

The interaction between the two methods can be split into two categories; long range electrostatic interaction and short range spatial interactions which are only relevant over small distances.

As one can imagine with the abundance of QM methods available, the possibilities

are numerous when combining with one of the, also, abundant MM methods. Such combined methods are collectively called QM/MM methods. Many QM/MM implementations exist and can be devided into roughly 3 categories.

- Extension of a QM program, *e.g.*
  - ONIOM in Gaussian03[1]
  - GAMESS-UK[2]
- Extension of a MM program, *e.g.*
  - AMBER[3]
  - CHARMM[4]
- A control program interfacing QM programs and MM programs, *e.g.*
  - CHEMSHELL[5]
  - QMMM[6]

Lin and Truhlar [14] review the most popular QM/MM methods in use today.

Our current work focuses on the long range interaction between the QM and the MM calculations. Potential due to each calculation is included in the other to achieve this long range interaction. The short range interaction will not be considered in this work.

A potential energy surface based on the single center multipole expansion of water to simulate bulk water is used as the MM part and plane-wave DFT as the QM part.

[1] http://www.gaussian.com
[2] http://www.cfs.dl.ac.uk
[3] http://ambermd.org/
[4] http://www.charmm.org/
[5] http://www.chemshell.org/
[6] http://comp.chem.umn.edu/qmmm/

3.2 Software Detail

3.2.1 DFT - STATE

STATE or "**S**imulation **T**ool for **A**tom **TE**chnology" is a program that performs DFT calculations and has been developed by Morikawa *et al.* [15]. The choice of this program came natural due to a cooperation formed between prof. Hannes Jónsson of the University of Iceland and associate prof. Yoshitada Morikawa of Osaka University. This meant that access to STATE's developers was easy.

Even though the methods used in this chapter were designed to be used with STATE, they should be easily transferable to most other DFT programs.

3.2.2 PES - SCME

SCME is a potential energy surface, PES, for bulk water based on the **S**ingle **C**enter **M**ultipole **E**xpansion [16], developed by Vila *et al.*

SCME was also mostly chosen out of convenience as access to its developers was readily available.

3.2.3 Compilation issues

Compiling SCME did not take much effort on all the clusters used, Itanium[7], Bjólfur[8] and Jötunn[9].

STATE was already available at Itaninum but not on the Icelandic clusters, Bjólfur and Jötunn. It proved quite problematic to compile STATE and was very time consuming.

At first the difference in architecture compared with Itanium, which is 64 bit while Bjólfur is only 32 bit, was suspected to be the culprit. This was, however, not the problem since we had the same problems on the newer cluster, Jötunn which is 64 bit.

[7] A computer cluster run by Yoshida lab at the University of Osaka, http://www.cmp.sanken.osaka-u.ac.jp

[8] http://hartree.raunvis.hi.is/~vidar/Bjolfur

[9] A computer cluster run by Reiknistofnun Háskóla Íslands, http://www.rhi.hi.is

After considerable attempts of replacing libraries and compilers we managed to compile STATE using ifort[10]/mkl[11].

There were still problems using this setup since test cases of more than 1 atom would crash once they reached the heavier calculational parts of STATE. After much thinking and debugging a solution was stumbled upon which worked for both clusters. The stack size of the linux shell had to be set to unlimited to handle the calculations.

3.3 Long Range Potential Interaction

3.3.1 Including an external potential in DFT calculations

DFT Unit Cells

In DFT calculations which are expanded in plane waves the system is sets up defined by a bounding box. This is called a unit cell. The unit cell is then repeated identically in each of the three directions infinitely often. Because of this the unit cell must have periodic boundary conditions, otherwise values could go to infinity as the unit cell is reapeated.

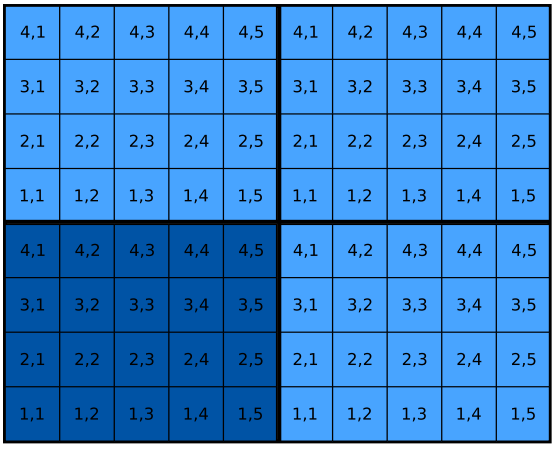

Figure 3.1: A 2D diagram of a unit cell. The dark area is the main unit cell and the lighter areas are periodic images of the main cell. The coordinates show how the grid values of the unit cell are repeated in its images.

Any variable, A, that is defined cell wide, must have the same value at the edges of the cell,

$$A(0) = A(L) \tag{3.1}$$

where L is the length of the cell in a given direction. This one dimensional constraint must hold for all edges of the

[10]http://www.intel.com/cd/software/products/asmo-na/eng/282048.htm
[11]http://www.intel.com/cd/software/products/asmo-na/eng/307757.htm

unit cell and all cell wide values. Furthermore the first derivative must also be the same at these edges.

DFT grids

Since it is impossible to store continuous values in computers, grids of discrete values must be used. In DFT calculations the information is stored discretely on 3 dimensional grids. This means that the unit cell is broken into small subsections. One point in the grid then represents each subsection. The grid must also satisfy equation 3.1. See figure 3.1 for a visual explanation.

Implementation

To include an external potential in the Kohn-Sham equations, equation 2.8, and thereby in the self-consistent electronic structure calculations, the external potential must be available on a unit cell of the same size as the DFT unit cell. The external potential must be on a grid with the same density as the effective potential v_{eff} in equation 2.10. Once this is the case it is quite simple to add the two. The external potential is thereafter included in the electronic calculations. This can either be done in real space or in Fourier space, where the grids might be more accessible. Note that this fails to take into account the contribution to the total energy of the nucleus due to the external potential,

$$E_{\text{Total}} = E_{\text{Electron}} + \sum_A Z_A v_{\text{ext}}(\mathbf{r}_A) \tag{3.2}$$

where v_{ext} is the external potential, Z_A is the charge of the nucleus and $\mathbf{r}_A$ is the location of each nucleus.

If Newtonian dynamics are to be preformed, it is important to realize that the above only gives the forces on the nuclei due to the electrons and their interaction with the external potential. Since DFT operates under the Born-Oppenheimer approximation the effect of the external potential on the nuclei must also be considered. To get a correction to the force provided by the electron calculations the force due to the external potential on each nucleus must be added:

$$\mathbf{F}_{\text{Total}} = \mathbf{F}_{\text{Electron}} + \mathbf{F}_{\text{ExtPot}} \tag{3.3}$$

where

$$\mathbf{F}_{\mathrm{ExtPot}} = Z_A \frac{\partial v_{\mathrm{ext}}}{\partial \mathbf{r}}\bigg|_{\mathbf{r}=\mathbf{r}_A}. \tag{3.4}$$

3.3.2 Including an external potential in multipole potential surface calculations

To see the effects of external potentials in calculations based on multipoles, it must be realized that the actual potential only affects the monopole and in the case of SCME the monopole is not included. Hence we only use derivatives of the potential. The dipole is affected by the electric field, the first derivative of the potential, and so on until the hexadecapole, the last multipole used in SCME, which is affected by the fifth derivative of the potential.

To include these effects in SCME, the appropriate derivative of the external potential is added to the corresponding internal derivative. This must be done in two places, first in the self-consistent induction calculations and secondly to the main self-consistent energy and force calculations.

The Induction Calculations

SCME consideres the polarizability of each molecule by calculating the induced dipole-dipole interactions, dipole-quadrupole interactions and quadrupole-quadrupole interactions. As such, the environment of each molecule is to some extent accounted for [10].

For each molecule, the components of the induced dipole, $\Delta\mathcal{P}$, and induced quadrupole, $\Delta\mathcal{Q}$, are defined as follows:

$$\Delta\mathcal{P}_i = \sum_j \alpha_{ij} E_j + \frac{1}{3}\sum_{j,k} A_{i,jk}\frac{\partial E_j}{\partial r_k} \tag{3.5}$$

$$\Delta\mathcal{Q}_{ij} = \sum_k A_{k,ij} E_k + \sum_{k,l} C_{ij,kl}\frac{\partial E_k}{\partial r_l} \tag{3.6}$$

where $\mathbf{E}$ is the electric field (the first derivative of the potential), α_{ij} is the dipole polarizability, $A_{i,jk}$ is the dipole-quadrupole polarizability and $C_{ij,kl}$ is the quadrupole-quadrupole polarizability. All the polarizabilities are tunable con-

stants. The indices; i, j, k and l, all represent each axial component; x, y and z.

To add the external potential to the induction calculations, the appropriate derivatives thereof, first and second respectively, are added to the E_i and $\partial E_i/\partial r_j$ elements respectively in equations 3.5 and 3.6. This must be done for each step of the self-consistent calculations since a new internal electric field is generated every step according to the change in dipoles and quadrupoles.

The Main Energy and Force Calculations

After the dipoles and quadrupoles have been induced it is simple to add each derivative of the external potential to the corresponding internal derivative since the internal values will not be recalculated hereafter.

3.3.3 Exporting the potential from the DFT calculation

In order to calculate the energy and the force on the water molecules described by SCME, every derivative of the potential up to and including the fifth is needed, as shown in section 3.3.2, at the centers of mass of each water molecule in the SCME region of the calculation. With the potential from the DFT calculation, the derivatives can be obtained quite easily. Calculating these derivatives, especially the higher ones, in real space can be quite cumbersome and inaccurate since numerical methods do not consider gridpoints that lie far away from the point at which the potential is being calculated. Therefore it is better to produce the derivatives in Fourier space, where every point in the grid is included and the calculations are reduced to simple multiplications.

Given the electrostatic potential, which is readily available from the K-S equations 2.8, the derivatives can be produced for each cartesian coordinate (x, y and z), labelled j,

$$\begin{aligned} \frac{\partial V(\mathbf{r})}{\partial r_j} &= \sum_{\mathbf{G}} (iG_j) V(\mathbf{G}) e^{i\mathbf{G}\cdot\mathbf{r}} \\ &\vdots \\ \frac{\partial^5 V(\mathbf{r})}{\partial r_{j1}\partial r_{j2}\partial r_{j3}\partial r_{j4}\partial r_{j5}} &= \sum_{\mathbf{G}} (iG_{j1})(iG_{j2})(iG_{j3})(iG_{j4})(iG_{j5}) V(\mathbf{G}) e^{i\mathbf{G}\cdot\mathbf{r}}. \end{aligned} \tag{3.7}$$

Using these derivatives, it is possible to either construct a grid in the SCME region and interpolate for the centers of mass or calculate for each center of mass directly.

When producing so many high level derivatives it most likely becomes necessary to maintain an unusually dense potential grid to get accurate results.

3.3.4 Exporting the potential from the multipole calculation

To produce the potential at location $\mathbf{r}$ due to the water molecules calculated by the multipole calculations, the contribution of each multipole is summed up,

$$\begin{aligned} V_{\mathcal{P}}^{m}(\mathbf{r}) &= \sum_{i} \frac{\mathcal{P}_i R_i}{|\mathbf{r}-\mathbf{r}'|^3} \\ V_{\mathcal{Q}}^{m}(\mathbf{r}) &= \sum_{i,j} \frac{\mathcal{Q}_{i,j} R_i R_j}{3\,|\mathbf{r}-\mathbf{r}'|^5} \\ V_{\mathcal{O}}^{m}(\mathbf{r}) &= \sum_{i,j,k} \frac{\mathcal{O}_{i,j,k} R_i R_j R_k}{15\,|\mathbf{r}-\mathbf{r}'|^7} \\ V_{\mathcal{H}}^{m}(\mathbf{r}) &= \sum_{i,j,k,l} \frac{\mathcal{H}_{i,j,k,l} R_i R_j R_k R_l}{105\,|\mathbf{r}-\mathbf{r}'|^9} \end{aligned} \tag{3.8}$$

where $V_{\mathcal{P}}(\mathbf{r})$, $V_{\mathcal{Q}}(\mathbf{r})$, $V_{\mathcal{O}}(\mathbf{r})$ and $V_{\mathcal{H}}(\mathbf{r})$ are the contributions to the potential at $\mathbf{r}$ due to the dipole, quadrupole, octopole and hexadecapole, respectively, of a single water molecule, m, whose center of mass is at $\mathbf{r}'$. The indices; i, j, k and l represent each axial component; x, y and z. $R_i = (r_i - r'_i)$ is used for simplification of the formulas.

To get the total potential at location $\mathbf{r}$, the contributions of all the multipoles in equation 3.8 are summed up and then the contribution of each molecule is summed over,

$$V(\mathbf{r}) = \sum_{m=1}^{N} \left[V_{\mathcal{P}}^{m}(\mathbf{r}) + V_{\mathcal{Q}}^{m}(\mathbf{r}) + V_{\mathcal{O}}^{m}(\mathbf{r}) + V_{\mathcal{H}}^{m}(\mathbf{r}) \right] \tag{3.9}$$

where N is the number of water molecules.

Using equations 3.8 and 3.9, the potential due to the water molecules in the SCME calculations can be produced at any location, in particular a grid of potential

values that is of the same size and density as the grid used in the DFT calculations.

3.4 Combined Calculations

The long range interactions between the two calculations are done by having the potential due to one system act on the other and then *vice versa*.

Both calculations, DFT and PES, are done using periodic unit cells, see figure 3.1. When setting up the unit cell for one of the calculations the other system must be taken into account. A vacuum must be included in each unit cell to account for the other calculation and minimize unwanted interaction of periodic images.

It should be stressed that no actual calculations were carried out and this section is only an analysis of what might happen.

3.4.1 Slab Calculations

A metal surface in water is a simple example of a setup that this method could simulate.

A thin layer of metal atoms, a slab, is set up and water placed on top of it in the DFT calculation, the remaining bulk water is then treated by the PES. Interactions between the slab/water and bulk water are then done via the potential due to each system.

When setting this up, a vacuum in the direction normal to the surface of the slab must be included in the DFT calculation and in the PES calculation a vacuum which accounts for the slab from the DFT calculation. Since this vacuum is different for each calculation the choice of unit cell becomes important.

Equal Size Cells

Choosing the unit cell of both calculations to be the same is useful in a number of ways but has its disadvantages as well.

Using equal size unit cells results in a total system that is easy to visualize. Each cell can be superimposed on the other to produce a complete image of the complete system.

The calculation of potential and derivatives thereof in the PES region becomes easy since the DFT grids extend over the whole PES cell. However, this poses the problem that large cells in DFT calculations can be calculationally very heavy.

Different Size Cells

By choosing different cell sizes some advantages appear as well as some disadvantages.

The cell sizes are independant and can therefore be optimized seperately. The cell size can generally be chosen smaller than with the equal size cell which results in easier calculation.

Since the DFT grids will not extend to the entire PES region a different method for evaluating the potential and derivatives must be employed. A good candidate is the multipole expansion.

3.5 Short Range Interactions

Generally there will be a zone where the interaction needs to be described more fully than by potential interaction. This zone is at the interface between the 2 calculations.

A method that might seem straight forward is to have both codes calculate the atoms at the interface. The forces on the interface atoms can then be calculated as a linear combination of the two calculations. One or both programs might impose some restrictions on the molecules so these restricitions might need to be considered. In the case of SCME the water molecules are rigid. The linear combination of forces would have to consider this when calculating the total force.

Our work did not cover these short range interactions at all and therefore we shall not discuss them further.

3.6 Summary

We have presented the basis of a method to extend DFT calculations using a potential energy surface. In particular we have included the necessary formulas to extend STATE [15], a DFT program, with SCME [16], a PES that employs the single center multipole expansion. The methods in this chapter only cover the long range interactions which are done by having the potential due to one calculation interact with the other as described in section 3.3. The short range interactions are outside the scope of the current work.

The compilation troubles described in section 3.2.3 had profound influence on this project. They along with various other reasons resulted in the abandonment of the project in favor of the work described in chapter 4. The experience in dealing with external potentials within the DFT framework was, however, not lost since the later work deals directly with the effect of external potentials in DFT calculations.

Chapter 4

Mimicking the Electrode Potential Profile of a Charged Solid-Liquid Interface with External Potentials

4.1 Introduction

Understanding the charged solid-liquid interface of electrochemical systems has been an active field for over 150 years, dating back to Hermann von Helmholtz in 1853 [17]. Ever since then, models of the interface have been formulated, *e.g.* [18, 19, 20, 21, 22].

The ion distribution and the effective potential, *i.e.* electrode potential profile, of an electrochemical system are schematically shown in figure 4.1.

When the potential bias is tuned in an electrochemical cell, the electrons are forced to move from one electrode to the other, making the electrodes oppositely charged. The charged surfaces form a double layer [23] with the ions coming from the electrolyte and thereby screening the electrode's charge from the rest of the liquid. At first the effective potential changes rapidly since most of the ions are located near the surface. However, as distance from the surface becomes greater and fewer ions exist in the electrolyte the potential changes with an exponential decay.

The methods of ab initio calculations, which have been very important for the present understanding of the gas-solid interface, have only been applied recently

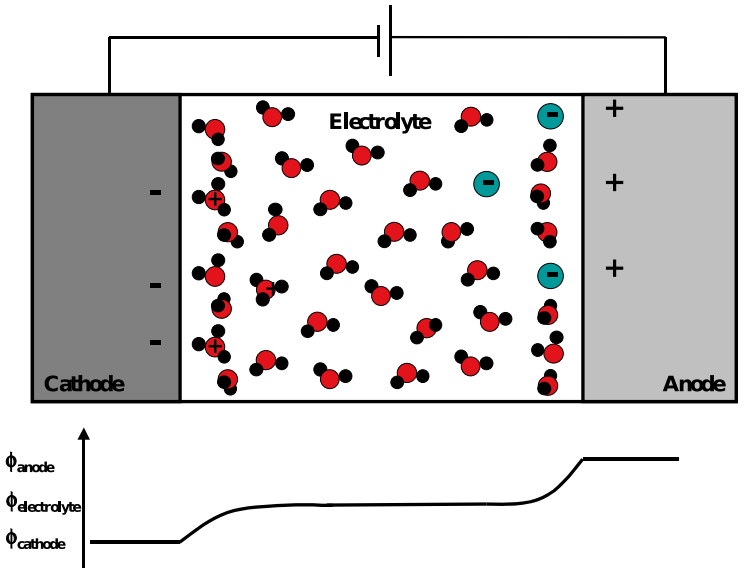

Figure 4.1: A real electrochemical system with 2 electrodes and an electrolyte in-between. Below the effective potential in the cell is shown. Printed with permission [24].

for the charged solid-liquid interface [25, 26, 27, 28, 29]. These recent models consist of periodic DFT or molecular dynamics calculations in the attempt to mimic the double layer. Taylor et al. review some of these recent models in their article from 2006 [26].

Sugino *et al.* [28], see figure 4.2(a), remove charge from the system and then re-insert it slowly while performing dynamics. This results in a charge buildup in the metal while the countercharge resides in an effective screening medium (ESM) [27]. As can be seen the effective potential rises quickly near the two charged layers of the electrode-water and the water-ESM interfaces. This is due to a rearrangement of the water molecules, not because the countercharge is located at the right place in the solid-liquid interface. In addition there is a small electric field throughout the water.

Skúlason *et al.* [29], see figure 4.2(b), insert a hydrogen atom in the water bilayer at the surface. When solving the electronic structure it forms a hydronium ion (H_3O^+) and surrenders most of its charge to the metal surface. This creates a double layer with the right features. However, as the counter ions are explicitly right outside the metal, the double layer dies out too quickly and lacks the exponential decay that should be present further away.

Filhol *et al.* [25], see figure 4.2(c), insert extra charge into the system which

gathers in the metal. A homogeneous countercharge is then applied to the whole system to maintain charge neutrality. This results in a smeared out double layer.

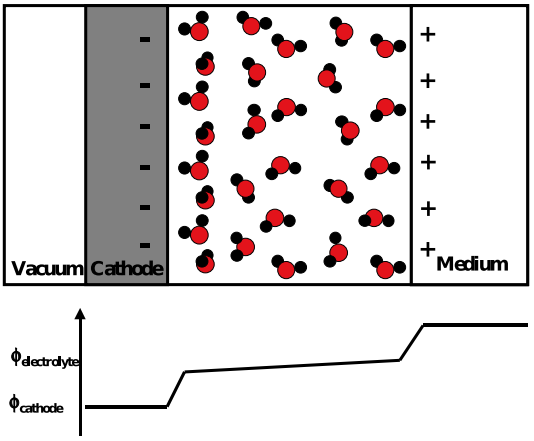

(a) Sugino *et al.* [28].

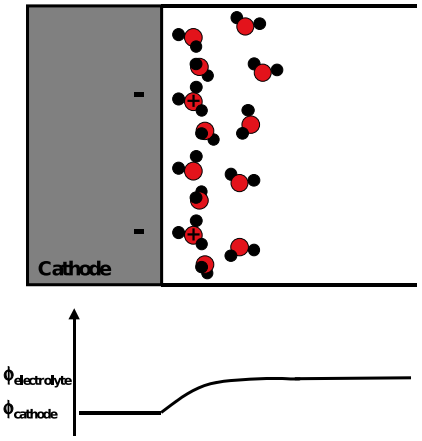

(b) Skulason *et al.* [29].

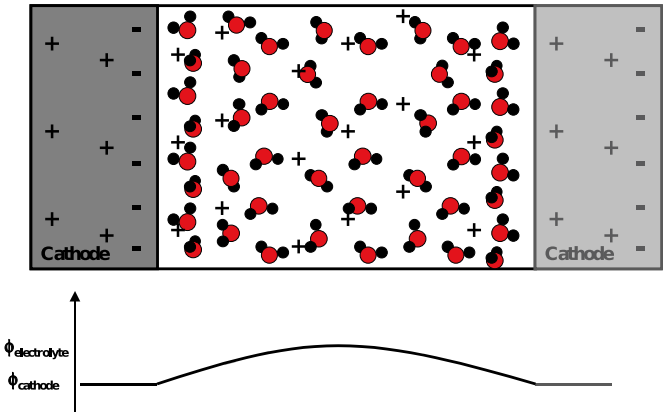

(c) Filhol *et al.* [25].

Figure 4.2: Setups and effective potentials for recent electrochemical systems. Printed with permission [24].

4.1.1 Electrochemical cells

An electrochemical cell consists of 2 half-cells, an ion bridge and a wire. Each half cell consists of an electrode and an electrolyte which surrounds the electrode. Surrounding the charged electrodes the electrolyte reacts to form a double layer by bringing particles of the opposide charge close to the electrode and thereby screening the charge of the electrode somewhat to the rest of the electrolyte.

The electrodes are connected with the wire through which the electrons flow while the electrolytes are connected with the ion bridge to allow for free flow of ions between the 2 half-cells [30]. See figure 4.3(a) for a graphic representation.

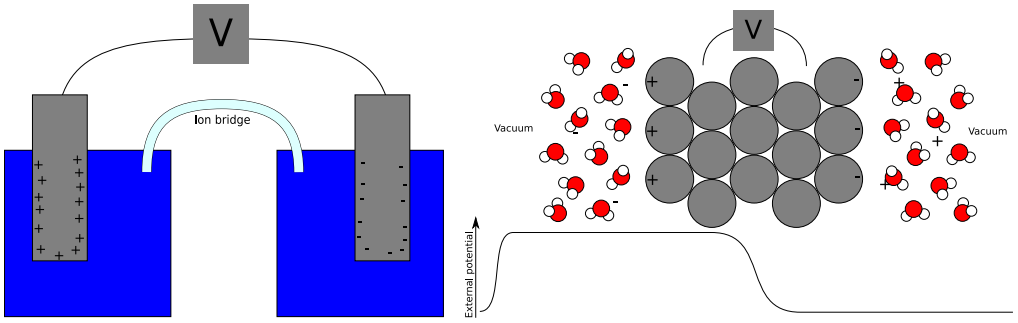

(a) A classical electrochemical cell.

(b) Our electrochemical cell model which has a one-to-one correspondence to the classical electrochemical cell shown in (a).

Figure 4.3: Our model shown in comparison to a classical electrochemical cell.

We suggest this system can be simulated using only a thin film of metal atoms (a slab) and an external potential to manipulate the electrons. By having the top layer of the slab with less potential than the bottom layer, electrons should migrate from the bottom layer to the top layer. With this setup the top layer acts as the negatively charged electrode, the bottom layer as positively charged electrode, the layers in-between as the wire and the external potential as the potential difference of the classical electrochemical cell. Compare figures 4.3(a) and 4.3(b) for a graphic explanation. Since the DFT cell is periodic in the direction normal to the slab surface, as well as the other directions, the space between the slab and its virtual image in the direction normal to the electrode surface can be filled to represent the electrolytes and the ion bridge.

By applying this external potential to a full system of a slab and water, the water should re-align to form a double layer with the slab that looks similar to the real one as seen in figure 4.1.

Our model offers a one-to-one correspondence of each part of the real system and is therefore easy to understand and could be used to simulate a whole electrochemical cell in one DFT calculation.

4.2 Software & Calculational Details

4.2.1 DFT

Dacapo[1] is a DFT calculator that plugs into the ASE2[2] python interface. This setup was chosen for the DFT calculations due to previous familiarity with its capabilities. In particular it was known that external potentials could be included in the calculations. The method of inclusion is similar to the method described in chapter 3.

The electronic structure problem is solved using density functional theory in a plane wave pseudopotential implementation [31, 32], employing ultrasoft pseudopotentials [8] to represent the ionic cores. All calculations were performed using the RPBE exchange-correlation functional [7] unless otherwise stated. The self-consistent electron density is determined by iterative diagonalization of the Kohn-Sham hamiltonian, with the occupation of the Kohn-Sham states being smeared according to a Fermi-Dirac distribution with a smearing parameter of $k_BT = 0.1eV$. In general a dipole correction [33] is not used, however, its effect will be discussed in section 4.3.4. In all the calculations the planewave cutoff is set at $26Ry$ and the density cutoff at $26Ry$, however, for caluclations that were Bader analysed the density cutoff was set to $86Ry$ to obtain a denser grid. When structures were relaxed the force tolerance was set to $0.01eV/\AA$ unless otherwise stated.

4.2.2 Compilation of Dacapo

As with the work in chapter 3, severe compilation problems plagued this part of the project. Both Dacapo's fortran code and ASE's python code were problematic. Problems with libraries and external python modules were prominent as well as the stability of the fortran code. We needed to be particularly careful regarding stability and network traffic as a previous installation of Dacapo had been prone to crash the entire cluster it was running on, Bjólfur[3]. Such a crash would leave the cluster inoperable for a day or even a few days due to possible data corruption on the data server.

[1] An open source code, available at http://wiki.fysik.dtu.dk/dacapo
[2] An open source code, available at http://wiki.fysik.dtu.dk/ase2
[3] http://hartree.raunvis.hi.is/~vidar/Bjolfur

The probelm with network traffic seemed to be unique to Bjólfur and could be circumvented by only writing the huge binary data file[4] to a scratch disk during the calculation while writing trajectories to the main data server. This method has the drawback that the binary data files are lost and to display things such as electron density, effective potential, etc. one needs to converge the electron calculations from the last postitions in the trajectory again, starting from a random wavefunction, now with the binary data file written to the main data server.

As for compiling, ifort[5] was our first choice, along with its libraries, MKL (**M**ath **K**ernel **L**ibrary)[6]. However, after running into problems with ifort when compiling the NetCDF libraries[4], we were forced to try GNU compilers[7] instead.

GotoBLAS[8] with GNU compilers have been shown to perform better than basic BLAS and even close to the performance of ifort/mkl [34], so they were a natural choice for BLAS(**B**asic **L**inear **A**lgebra **S**ubprograms) libraries [35]. However, after considerable difficulty in compiling GotoBLAS, we reverted to a more basic BLAS[9].

This compromise might have slowed the program down but no such tests were conducted and the program used as such.

4.2.3 Differentiable External Potential Function

We have written a module to produce external potentials on a grid in the Python programming language. The Python language was the obvious choice since the DFT program uses a Python interface, ASE. Our calculations require us to use a potential which is static in 2 directions (x and y) but tunable in the last direction (z). In effect our python program produces a 1 dimensional potential grid which is then extended to the other 2 dimensions.

The 1D potential is a combination of 4 polynomials, 2 of which are of the first degree and 2 of which are of the third degree in alternating order. The external

[4]http://www.unidata.ucar.edu/software/netcdf
[5]http://www.intel.com/cd/software/products/asmo-na/eng/282048.htm
[6]http://www.intel.com/cd/software/products/asmo-na/eng/307757.htm
[7]http://gcc.gnu.org/fortran
[8]http://www.tacc.utexas.edu/resources/software
[9]http://www.netlib.org/blas/index.html

potential in whole obeys the same boundary conditions as the DFT calculations and is differentiable in all points.

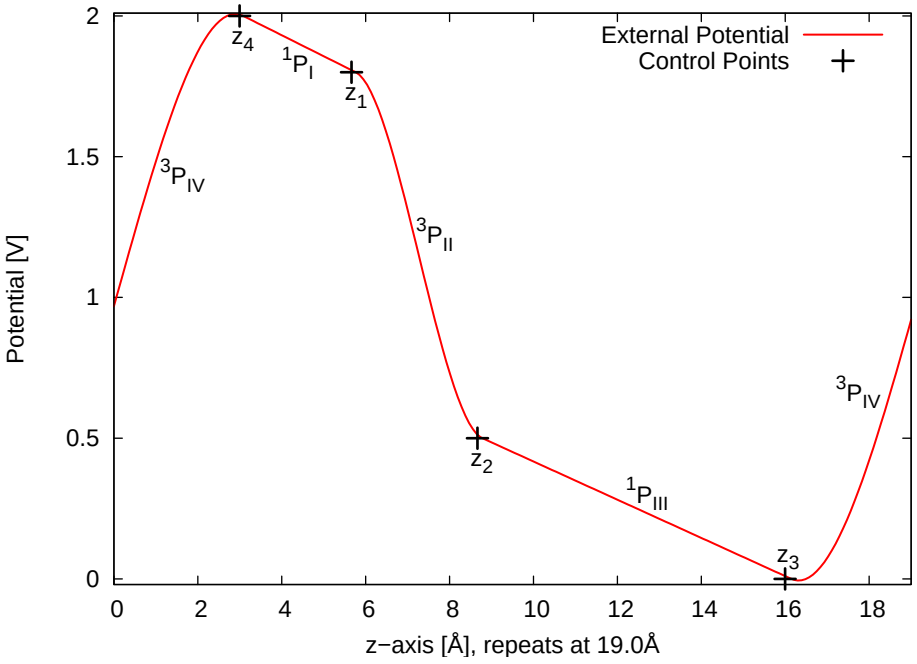

Figure 4.4: A sample polynomial showing the control points and different parts of the polynomial. This 1 dimensional potential can then easily be extended to be invariant in the directions parallel to the metal surface.

The parameters that control the potential are the 4 points where different polynomials meet.

The 1° polynomials are created simply by making a straight line between the control points while the 3° polynomials are defined by the following equations:

$$\begin{aligned} {}^3P_{II}(z_1) &= {}^1P_I(z_1) \\ {}^3P_{II}(z_2) &= {}^1P_{III}(z_2) \\ \left.\frac{d^3P_{II}}{dz}\right|_{z=z_1} &= \left.\frac{d^1P_I}{dz}\right|_{z=z_1} \\ \left.\frac{d^3P_{II}}{dz}\right|_{z=z_3} &= \left.\frac{d^1P_{III}}{dz}\right|_{z=z_3} \end{aligned} \tag{4.1}$$

where ${}^3P_{II}$, ${}^1P_I$ and ${}^1P_{III}$ are the 3° polynomial in interval II, 1° polynomial in interval I and 1° polynomial in interval III respectively. See figure 4.4 for a graphic explanation.

With equations 4.1, $P^3_{II} = a_{II}z^3 + b_{II}z^2 + c_{II}z + d_{II}$ can be easily solved for a_{II}, b_{II}, c_{II} and d_{II} using equations 4.1 as constraints for a system of 4 equations.

P_{IV}^3 is created in a similar manner.

We now define half the length of each 3° polynomial as its smearing. This term becomes important when applying the potential on an actual system as we will show in section 4.3.3.

4.2.4 Calculational Setup

Our system is composed of a platinum 111 slab, using a lattice constant of 4.02$\mathring{A}$, with varying number of atoms. Each layer is in a 3x2 configuration, while the number of layers is variable. The number of layers will be discussed further in section 4.3.3. We then have an external potential act on the slab in such a way that each side of the slab has a different potential with a drop in potential in the middle of the slab and a rise in the vacuum. Outside of the drop and rise the potential is constant. This potential setup will hereafter be referred to as the U-potential. For a graphic explanation see figure 4.5.

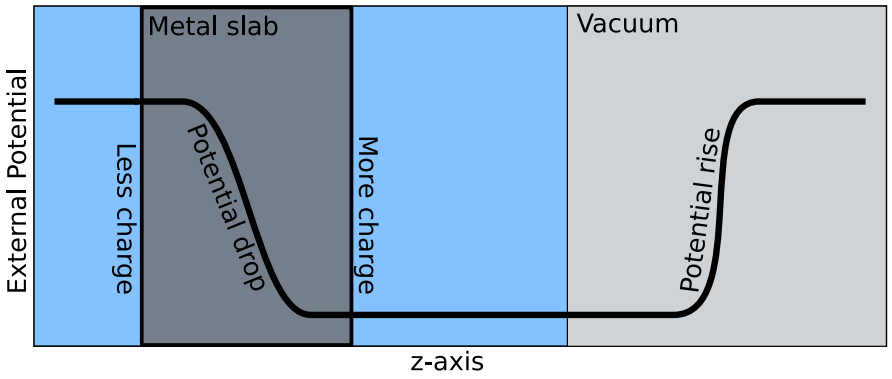

Figure 4.5: A diagram showing how the U-potential is set up.

On each side of the slab we then add what is needed for each particular calculation. In the case where there is nothing but the slab in the calculation we use a perfect crystal structure for the entire slab. When water is included in the system, the top layer of the slab has been relaxed along with the water.

4.3 Results and Discussions

4.3.1 Terminology

A concept that will be used a lot in this section is electron density difference, $\Delta\rho_{xy}(z)$. This concept describes the electron density, $\rho(\mathbf{r})$ of a system, compared to a different system, averaged over the x- and y- directions. In general a system that has external potential applied to it will be compared to a system that has no external potential applied to it. The atomic configuration of both systems is the same so the effect of the external potential can be extracted.

All the values that DFT deals with are discrete so the math becomes quite simple:

$$\Delta\rho(\mathbf{r}) = \rho_{\text{ExtPot}}(\mathbf{r}) - \rho_{\text{Neutral}}(\mathbf{r}) \tag{4.2}$$

and

$$\Delta\rho_{xy}(z) = \frac{\sum_{x,y}\Delta\rho(\mathbf{r})}{n_x n_y} \tag{4.3}$$

where n_x and n_y are the number of grid points in the x- and y- directions respectively.

Another concept used is the effective potential, $\Delta V_{xy}(z)$, which represents the change in electrostatic potential compared with a system without external potential applied. This is defined in the same manner as above

$$\Delta V(\mathbf{r}) = V_{\text{ExtPot}}(\mathbf{r}) - V_{\text{Neutral}}(\mathbf{r}) \tag{4.4}$$

and

$$\Delta V_{xy}(z) = \frac{\sum_{x,y}\Delta V(\mathbf{r})}{n_x n_y} \tag{4.5}$$

4.3.2 Electron Transfer

Initial tests confirmed the presence of an electron transfer effect. Using a simple setup, a 3 layer platinum slab that is subject to the U-potential, electrons move from the side which has higher potential to the lower potential side. This effect can be seen in figure 4.6.

It is also interesting to see that the effective potential is quite different from the

external potential in the areas without electrons. Instead of correcting for the periodicity of the cell deep in the vacuum in a abrupt change, this change is smoothed out over the whole region that is void of electrons and thereby forms an electric field in the vacuum.

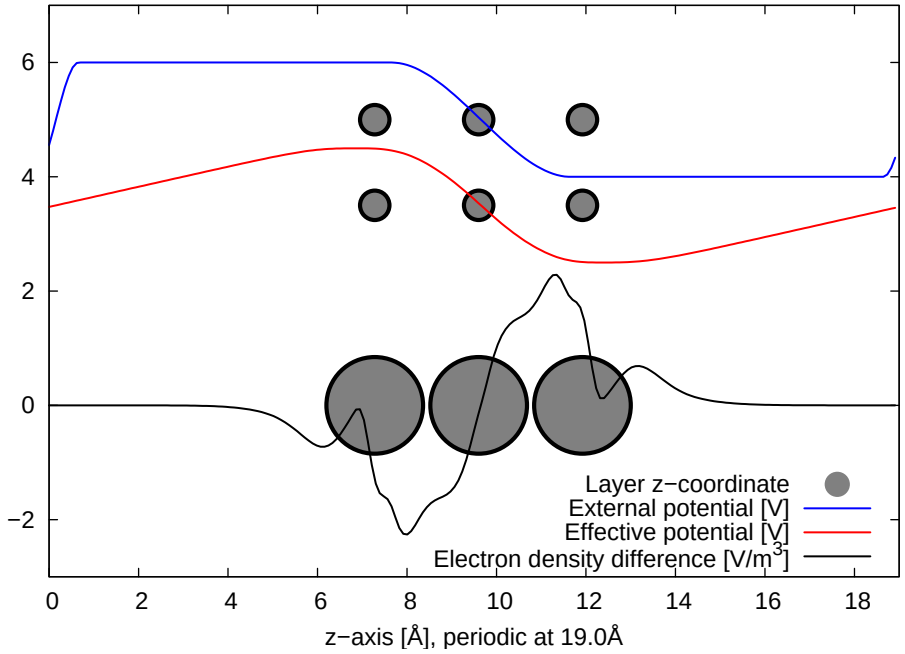

Figure 4.6: The setup of the system, the external potential that is applied (the U-potential), the effective potential and the difference in electron density compared with a system without an external potential applied. The potential profiles have been shifted upwards by $3.5V$ and $5.0V$ respetively and the electron density difference has been magnified by $1000x$.

Three main electron transfer effects are seen.

- The most obvious effect is the electron transfer which happens within the slab, two anti-symmetric tops, one representing deficiency of electrons and the other abundance of electrons. This effect will hereafter be referred to as the **in-slab** transfer.
- The second effect is the one we are most interested in, two anti-symmetric tops, one above the slab and one below. These represent the transfer of electrons from one side of the slab to the other. This effect will hereafter be referred to as the **side-to-side** transfer.
- The last effect is oscillations in the electron density between the previous two effects. This is not very visible when using such a thin slab but will be seen more clearly in section 4.3.3.

We believe the in-slab transfer is produced by the drop of the potential in the slab and is therefore purely an artifact of the calculational method. This is further discussed in section 4.3.4. On the other hand the side-to-side effect is due to the different potentail of each side of the slab which is what our method predicts.

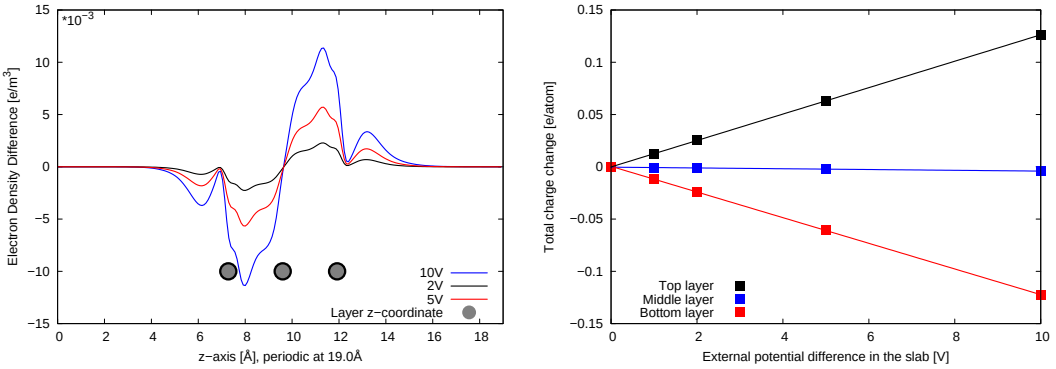

(a) Charge Density Difference.

(b) Bader Analysis.

Figure 4.7: The difference in electron density between a system that is subject to various potential drops in the slab compared to a system without any external potential applied, always using a 2.0Å smearing.

By applying different potential differences between the top and bottom slab layers, one can increase or decrease the electron transfer. Bader analysis, figure 4.7(b), shows this for the side-to-side transfer more clearly then simply plotting the difference in electron density, figure 4.7(a), and furthermore shows that the potential drop and the electron transfer are linearly dependant. Note that that Bader analysis cancels out the in-slab transfer completely for symmetric systems because symmetric systems produce anti-symmetric electron density difference. However if the system is not completely symmetric this anti-symmetry is broken. If the layers over which the potential drops are symmetric, as they are in our calculations for the most parts, the in-slab transfer is still almost anti-symmetric.

4.3.3 The Effect of Smearing and the Slab Size

After seeing the huge in-slab transfer within the slab in section 4.3.2, it is safe to assume that it might interfere with the main side-to-side transfer if the smearing is too large or the slab too thin.

If we look at the electron density of a given 3 platinum layer system which is

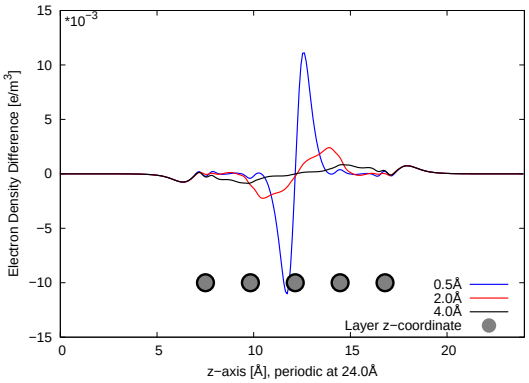

Figure 4.8: Comparison of the charge density difference of a system that is subject to a $2V$ drop in the slab. Each line represents a different smearing value.

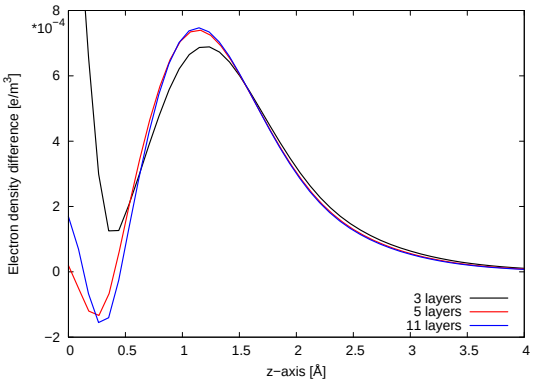

Figure 4.9: The electron density difference, closely above the slab. The top layer is set at $0.0\mathring{A}$. The smearing is set at $2.0\mathring{A}$ for all slabs and the drop is $2.0V$.

subject to the U-potential with varying smearing and compare with the same system without an external potential applied, we see that the side-to-side transfer is similar for different smearings while the electron density in the inner layer is quite different for different smearings.

When the number of platinum layers is increased to 5, the above effect seen more clearly, see figure 4.8. There is considerable electron transfer within the slab but with a small enough smearing the effect outside the slab is the same for all smearings. Larger smearings decrease the in-slab transfer so it becomes apparent that one must strike a balance between large in-slab transfer and convergence in the side-to-side transfer. Bader analysis confirms that the side-to-side transfer is the same for all smearings that are sufficiently small.

We choose to use 5 layers with the potential dropping over slightly less than the inner 3 layers, using a smearing of 2Å, for the bulk of our calculations. With this setup we manage to limit the severity of the in-slab transfer while still being quite sure that the side-to-side transfer is not affected. There seems to be no reason to use a larger slab as can be seen in figure 4.9.

4.3.4 Dipole Correction and the Effect of Cell Size

By exposing a slab to the U-potential we are making the slab asymmetric by manipulating its electrons. Due to this an electric field is produced in the vacuum. A dipole correction [33] is a cell wide saw shaped potential that can be employed to counter this electric field.

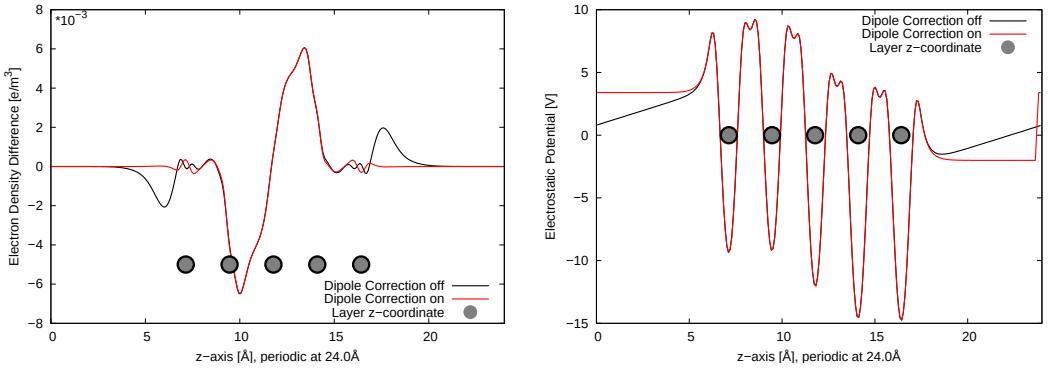

(a) Charge density difference.

(b) The electrostatic potential.

Figure 4.10: The U-potential is applied and we compare a normal setup to one with the dipole correction applied.

As figure 4.10 shows the dipole correction removes the side-to-side transfer by applying a saw potential that counters the electric field in the vaccum. The dipole correction, however, leaves the in-slab transfer intact which is consistent with our claim that the in-slab transfer is only due to the potential drop in the slab, since a simple saw potential would not even out the comparatively abrupt drop in potential that takes place in the slab. Figure 4.10(b) shows that the electrostatic potential changes dramatically in the vacuum when a dipole correction is applied. The electric field in the vacuum is removed by making the potential flat except in the middle of the vacuum where the potential changes abruptly to maintain periodicity.

Adding a dipole correction somewhat simulates a cell with an infinitly large vaccum, at least when considering the electric field. Then, how is the side-to-side transfer dependant on the size of the vacuum and thereby the electric field therein?

As figure 4.11(a) clearly shows, the side-to-side transfer depends on the size of the cell. Furthermore, Bader analysis of the data, figure 4.11(b), shows that the side-to-side transfer depends linearly on the electric field in the vacuum. Therefore

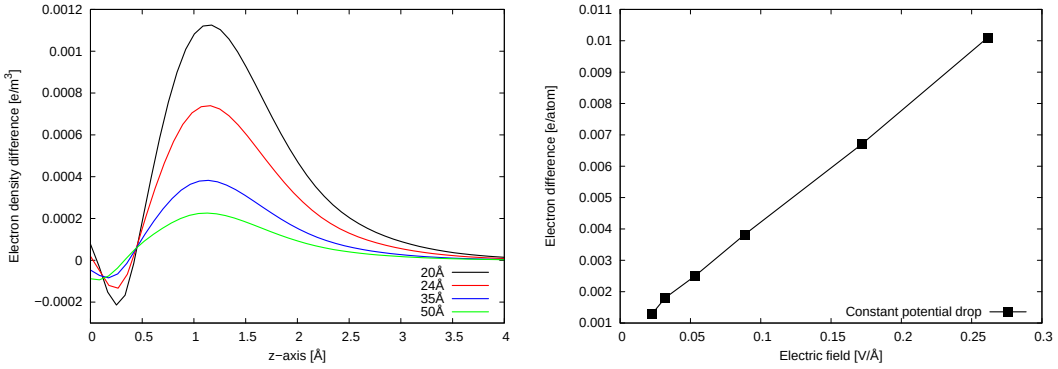

(a) The charge density difference compared to a system without external potential right above the slab. The top layer of the slab is at $0.0\mathring{A}$. Each line represents a different size cell.

(b) Bader analysis of the data in (a), shown as a function of the effective electric field in the cell's vacuum. Each point, therefore, represents a different cell size.

Figure 4.11: The same potential drop is applied to different size cells, by only varying the vacuum length but keeping the potential drop at $2V$ and smearing at $2.0\mathring{A}$.

it is clear that if the electric field is constant while varying the vacuum size and potential drop the side-to-side transfer will remain constant. We discuss this further in section 4.3.5.

It should be noted that vacuum size does not change the in-slab transfer at all. This is consistent with our previous observations regarding the dipole correction.

4.3.5 Comparison to a Saw Tooth Potential

Saw Tooth Potential Setup

A saw tooth potential (sometimes called a ramp potential) is a constant and even drop in potential with an abrupt rise at a given location to ensure periodicity. The main identity of a saw tooth potential is its uniform decrease (or increase) in potential. This creates an even electric field everywhere in the cell except where the abrupt rise is. This drop is generally placed in the middle of the vacuum and therefore doesn't affect the system in question if the vacuum is large enough.

The saw tooth potential has been used to simulate the Helmholtz layer[18] in a metal/water system, *e.g.* by Karlsberg *et al.* [36]. In this case the saw potential is set up to approximate the Helmholtz layer formed by the surface of the metal and the water by setting up an even electric field in the whole cell. The field

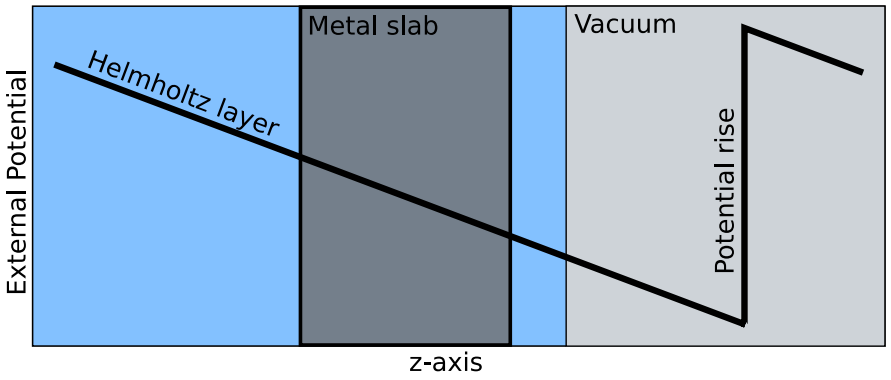

Figure 4.12: The saw tooth potential setup. The Helmholtz layer is displayed and the abrupt potential rise in the vacuum.

in the Helmholtz layer can be quite large, up to $0.5V/\mathring{A}$ [37]. Even though the actual Helmholtz layer should only be small, approximately $3\mathring{A}$ [37], the saw tooth potential does not allow this and sets up the electric field in the whole cell. This leads to a very large change in the vacuum where the periodicity is enforced.

Besides simulating the Helmholtz layer, this electric field produces a similar effect as our U-potential by transporting electrons from the slab side that has the higher potential to the lower potential slab side. This is problematic when using the saw tooth potential since the electrons will be transferred away from the surface that should be negatively charged according to the setup of the Helmholtz layer. This is a serious problems that the saw tooth potential suffers when used in electrochemical applications.

Simple slab

Once again we use a simple platinum slab that consists of 5 layers. We compare the application of 2 different external potentials; our U-potential and the saw potential described above. Both employ an abrupt change in the middle of the vacuum to maintain periodicity. This abrupt change is the same for both potentials in every system we compare.

We see from figure 4.13(a) that the electron transfer is quite similar in between the two methods outside the slab. On the other hand within the slab the situation is quite different. For this reason, Bader analysis shows slightly less electron transfer to the top layer under the saw tooth potential. However, as figure 4.13(a) shows the main side-to-side transfer, outside the slab, is almost identical in between

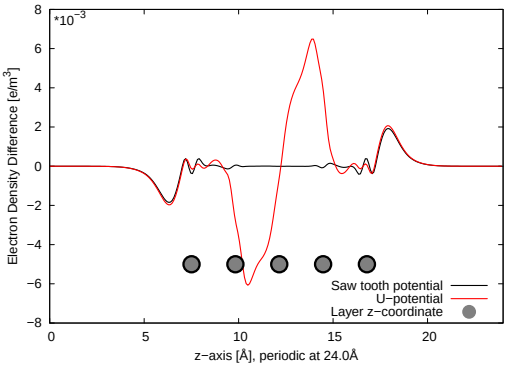

(a) Charge density difference.

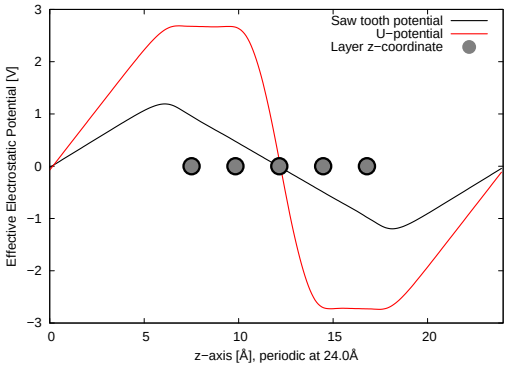

(b) Effective electrostatic potential.

Figure 4.13: A comparison of the U-potential and the saw tooth potential.

both methods.

As we showed in section 4.3.4, it is the electric field in the vacuum that controls the side-to-side transfer. Therefore it is quite interesting to see how completely different electric fields, see figure 4.13(b), produce very similar side-to-side electron transfer.

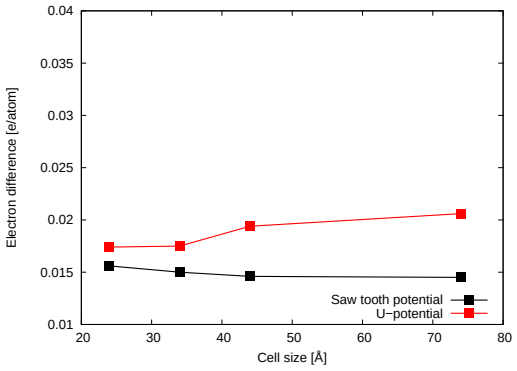

(a) The electric field of the U-potential is kept constant by varying the vacuum size and potential drop accordingly, shown as function of the cell size. The same parameters are then applied to the saw tooth potential calculation.

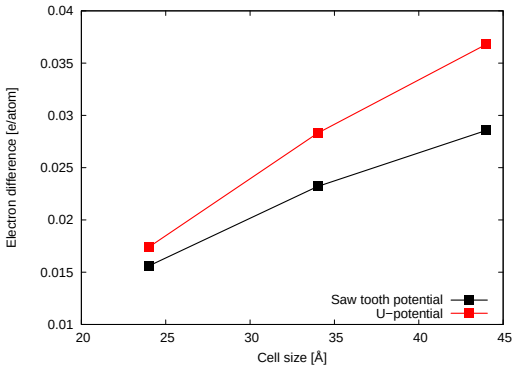

(b) The electric field of the saw tooth potential is kept constant by varying the vacuum size and potential drop accordingly, shown as a function of the cell size. The same parameters are then applied to the U-potential calculation.

Figure 4.14: Comparison of the charge change in the top layer of the slab using Bader analysis. The dependance of the charge transfer on the electric field in the vacuum of each method is explored.

In figure 4.14, we compare the effect of keeping the electric field in the vacuum constant while modifying the cell size and potential change in the vacuum. When

the electric field of the U-potential is kept constant and those parameters applied to both the saw tooth potential and the U-potential, the electron transfer is constant for different cell sizes, as seen in figure 4.14(a). On the other hand if the parameters from when the saw tooth's electric field is kept constant, are used the electron transfer changes for both methods, as seen in figure 4.14(b).

It is, therefore, clear from figure 4.14, that the side-to-side electron transfer for both potential setups depends on the potential change in the vacuum and the vacuum size. These sizes are characerized in the effective electric field in the vacuum of the U-potential calculation. This is peculiar in the case of the saw tooth potential since the effective electric field in the vacuum is very different from that of the U-potential, see figure 4.13(b). In this way the U-potential describes what is happening more clearly than the saw tooth potential.

Slab with one water molecule on top

As the surface of a slab gets more negatively charged, a water molecule on top of that slab turns the oxygen's lone pairs away from the slab and towards it when the surface gets more positively charged. We can use this effect to further compare the saw potential to our U-potential by using both to transfer electrons from the bottom layer of the slab to the top and comparing the angle of the water molecule for each method.

It should be noted that the calculations of this system are done using the PBE functional [6] instead of RPBE like elsewhere in this chapter. This is due to the fact that the water molecule did not form any sort of bonding to the surface using the RPBE functional. We also used lower force tolerance, $0.005eV/\AA$, for the relaxation, since the effect being measured is so delicate.

Figure 4.15(a) shows even further that the side-to-side transfer is the same for the saw potential and the U-potential when using the same potential drop in the vacuum. Only slight differences are to be found in the angle between the water molecule and the surface and they can easily be explained by either calculation not being as completely relaxed as the other.

There is a slight, but consistent, difference in the binding energies of the water molecule to the surface. As the surface becomes more negatively charged the saw tooth potential offers slightly less bonding, $1.5 \times 10^{-3}eV$ for $-4.0V$ difference

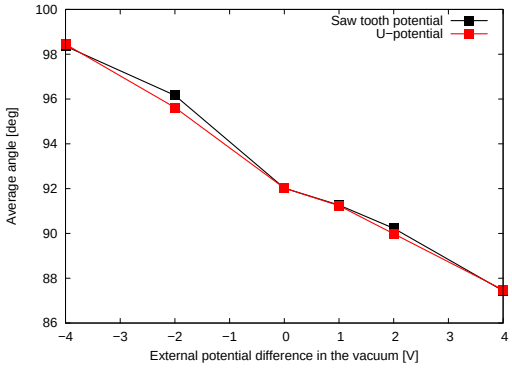

(a) The average angle as a function of the external potential change in the vacuum.

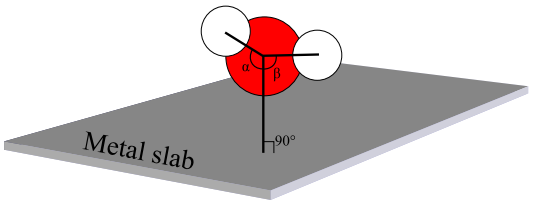

(b) A diagram showing how the angle between the water molecule and the platinum slab is defined with respect to the static plane of a layer of platinum.

Figure 4.15: Comparison of the angles between a water molecule and a platinum slab under the U-potential and the saw tooth potential. The angle shown in (a) is an average of the α and β angles shown in (b). Due to the setup of the system the top layer becomes more negatively charged as the voltage is more positive.

in the vacuum, than the U-potential. For a more positively charged surface the difference is the same but in favour of the saw potential. To measure such small energy differences, even lower force tolerances might be needed, larger external potential drops would be helpful and more points essential. However, the difference was consistent and linear, albeit small, for all measured values of the external potential drops.

4.4 Further Applications

Towards the end of this project an idea surfaced to extend our model beyond the manipulation of the metal's electrons. We saw prospect in imitating the actual effective potential profiles using external potentials.

One example of this is to mimic the double layer more fully than with the saw tooth potential. Both by forcing electrons into the correct slab side instead of out of it and also by giving a more full description of the double layer than the simple Helmholtz layer.

A few simple tests were performed using work by Rossmeisl *et al.* [38] as a rough guideline for the shape of the potential. Still using the function described in

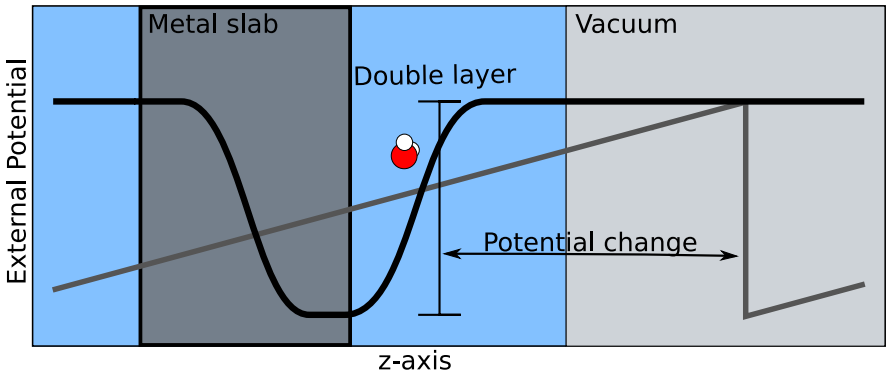

Figure 4.16: A diagram showing how the U-potential can be modified to produce an external potential that looks like a double layer close to the slab's surface. The saw tooth potential is shown in comparison and the potential change in each is defined. Note that the definition of the saw potential has changed.

section 4.2.3 to produce the external potential we simply moved the rise that used to happen deep in the vacuum to just above the surface of the metal. We then set it to look similar to their double layer by setting the smearing at $2.5\mathring{A}$. See figure 4.16.

As a test case we repeated calculations from section 4.3.5 but using the modified U-potential. Figure 4.17 shows that with increasingly steep electric fields in the double layer region the angle is affect in the same way with both the modified U-potential and the saw potential. However, change is more with the modified U-potential. This is to be expected since by definition of the external potentials, the same voltage value does not give the same change in potential in the double layer region.

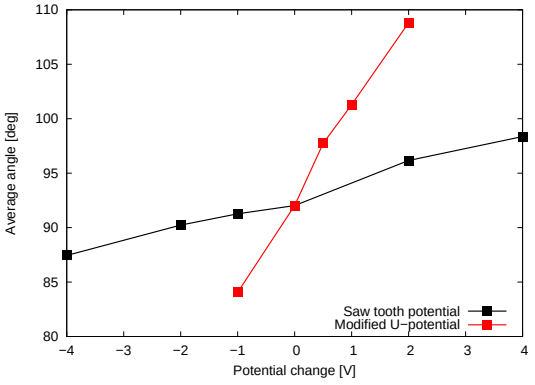

Figure 4.17: Comparison of the angles between a water molecule and a platinum slab using the modified U-potential and the saw tooth potential. The angle shown is the average of the angles show in figure 4.15(b). A more positive voltage gives a steeper electric field in the double layer.

If the size of the cell and the smearing of the double layer are compared it can be seen that a modified U-potential value of $0.5V$ is roughly equivalent to a saw tooth potential value of $3.5V$. This comparison seems to approximately match up. However, since this test was only

a primitive one, not too much significance should be put into the magnitude of the effect.

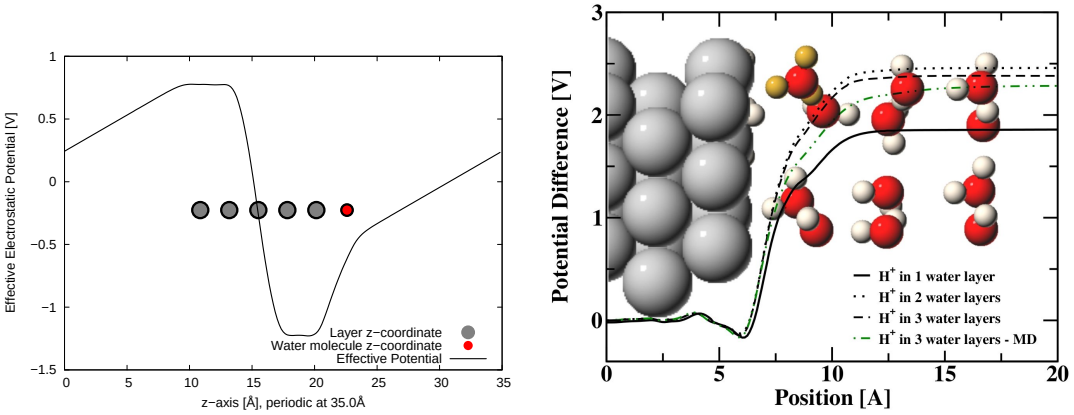

(a) The effective potential in a system of 5 platinum layers with one water molecule on top.

(b) The effective potential in a system calculated by Rossmeisl *et al.* [38]. Used with permission [24].

Figure 4.18: Comparison of a system that is affected by the modified U-potential and the system which was used to form the rough shape of the external potential.

In figure 4.18, the effective potential of the above system is shown in comparison to the work done by Rossmeisl *et al.* [38]. Even though these are not completely alike certain similarities are apparent. The most important similarities are between the slab and the water molecule where the effective potential rises almost identically. However, as we move further away from the slab and less electrons are present the potential forms an electric field to maintain periodicity.

Even though no exhaustive tests using this setup were performed we see great potential in its use. Simulation of surface chemistry with little water while the double layer is simulated using an external potential is perhaps the most obvious application, however, more testing of that setup is certainly needed.

To form a potential that better simulates the double layer, the external potential function from section 4.2.3 must be extended to allow more flexibility. In particular using a 3° polynomial in the double layer area will probably not be sufficient. In fact to produce a proper looking double layer, a large system that includes a double layer should be calculated without external potential and the external potential then fitted to the effective potential of that system.

4.5 Conclusions

We have presented a method to manipulate electrons near a metal slab. Setting the bottom and top layers of a slab at different potentials, by having the external potential change rapidly in the slab, pushes electrons to the lower potential side. This is useful to realistically simulate electrodes as they are in general either negatively or positively charged. Each side of the slab can then represent one electrode.

We have shown that charge is indeed pushed from one side of the slab to the other. Most importantly from just outside the higher potential side to just outside the lower potential side, we call this effect the side-to-side transfer. There is also charge transfer within the slab which we call the in-slab transfer.

We have shown that side-to-side transfer is directly dependant on the electric field in the vacuum. This field is formed to connect the unit cell to its mirror image and maintain periodicity in the potential. In a cell that only contains a slab, this field is characterized by the length of the vacuum and the potential difference. If the electric field is removed, *e.g.* by applying a dipole correction, the side-to-side electron transfer disappeares. To further study this behaviour a large system with a lot of water is needed. The water is used to screen out the effect of the electric field on the slab. However, such calculations were not carried out.

The in-slab transfer remains identical when exposed to various conditions under which the side-to-side transfer is affected. As long as the external potential changes over the same length, the in-slab transfer remains the same and is scaled with the potential drop in the slab. In particular the vacuum size has no effect on this in-slab transfer. After comparison with the saw tooth potential where there is no in-slab transfer but almost identical transfer from one side of the slab to the other, we believe it is safe to say that the in-slab transfer of the U-potential is purely an artifact of the calculation and as long as the external potential changes over a wide enough area and the slab is large enough to accomodate this, it will not affect the main side-to-side electron transfer.

In our comparison to the saw tooth potential an unexpected flaw in the saw tooth potential was discovered as the side-to-side transfer was dependent on the height of its periodic correction which happens deep in the vacuum and the size of the vacuum. This dependance turns out to be expressed in the effective electric field

of the U-potential and not the effective electric field of the saw tooth potential. This leads us to claim that the U-potential explains more clearly the side-to-side electron transfer of both methods.

The saw tooth potential is often used to simulate an electric double layer using a Helmholtz layer. By doing so, electrons are pushed away from the side that should be negatively charged. This is not a problem with the U-potential since it first moves the electrons to the correct side and then has the electrolyte react to form a double layer. Furthermore, the U-potential can be expanded to directly simulate the double layer by fitting an external potential to an actual double layer and thereby decreasing the need for heavy calculations using large quantities of water. This last setup was only suggested in this work and briefly looked at. It, therefore, needs more work to form a working method.

Bibliography

[1] Kohn, W. *Rev. Mod. Phys.* **1999**, *71*, 1253–1266.

[2] Pople, J. A. *Rev. Mod. Phys.* **1999**, *71*, 1267–1274.

[3] Hohenberg, P.; Kohn, W. *Phys. Rev.* **1964**, *136*, B864–B871.

[4] Kohn, W.; Sham, L. J. *Phys. Rev.* **1965**, *140*, A1133–A1138.

[5] Langreth, D. C.; Perdew, J. P. *Phys. Rev. B* **1977**, *15*, 2884–2901.

[6] Perdew, J. P.; Burke, K.; Ernzerhof, M. *Phys. Rev. Lett.* **1996**, *77*, 3865–3868.

[7] Hammer, B.; Hansen, L. B.; Nørskov, J. K. *Phys. Rev. B* **1999**, *59*, 7413–7421.

[8] Vanderbilt, D. *Phys. Rev. B* **1990**, *41*, 7892–7895.

[9] Batista, E. R.; Xantheas, S. S.; Jónsson, H. *The Journal of Chemical Physics* **1998**, *109*, 4546–4551.

[10] Batista, E. R.; Xantheas, S. S.; Jónsson, H. *Journal of Chemical Physics* **2000**, *112*, 3285–3292.

[11] Jackson, J. D. In *Classical Electrodynamics*, 2nd ed.; John Wiley & Sons, Inc., 1975; pp 1–143.

[12] Bader, R. F. W. *Atoms in Molecules: A Quantum Theory*; Oxford University Press: New York, 1990.

[13] Henkelman, G.; Arnaldsson, A.; Jónsson, H. *Comp. Mat. Sci.* **2006**, *36*, 354–360.

[14] Lin, H.; Truhlar, D. G. *Theoretical Chemistry Accounts* **2007**, *117*, 185–199.

[15] Morikawa, Y. In *"Simulation Tool for Atom TEchnology", in Introduction to Computational Materials Design – From the Basics to Actual Applications –*; Kasai, H.; Akai, H.; Yoshida, H., Eds.; Osaka Univ. Press, 2005; pp 54–72, 260–273.

[16] Vila, F. D.; Batista, E. R.; Jónsson, H. Unpublished Article "SCME: a Fast, Transferable H_2O Interaction Potential Based on a Single Center Multipole Expansion".

[17] Helmholtz, H. *Annalen der Physik und Chemie* **1853**, *165*, 211–233.

[18] Helmholtz, H. *Annalen der Physik und Chemie* **1879**, *243*, 337–382.

[19] Gouy, M. *Journal de Physique Théorique et Appliquée* **1910**, *9*, 457–468.

[20] Chapman, D. L. *Phil. Mag.* **1913**, *25*, 475.

[21] Stern, O. Z. *Elektrochem.* **1924**, *30*, 508.

[22] Grahame, D. C. *Chemical Reviews* **1947**, *41*, 441–501.

[23] Carnie, S. L.; Torrie, G. M. In *The Statistical Mechanics of the Electrical Double Layer*; Prigogine, I.; Rice, S. A., Eds.; John Wiley & Sons, 1984; Vol. 56, pp 141–253.

[24] Skúlason, E. Personal communication, 2008.

[25] Filhol, J.-S.; Neurock, M. *Angewandte Chemie International Edition* **2006**, *45*, 402–406.

[26] Taylor, C. D.; Wasileski, S. A.; Filhol, J.-S.; Neurock, M. *Physical Review B* **2006**, *73*, 165402.

[27] Otani, M.; Sugino, O. *Physical Review B* **2006**, *73*, 115407.

[28] Sugino, O.; Hamada, I.; Otani, M.; Morikawa, Y.; Ikeshoji, T.; Okamoto, Y. *Surface Science* **2007**, *601*, 5237–5240.

[29] Skúlason, E.; Karlberg, G. S.; Rossmeisl, J.; Bligaard, T.; Greeley, J.; Jónsson, H.; Nørskov, J. K. *Phys. Chem. Chem. Phys.* **2007**, *9*, 3241–3250.

[30] Zumdahl, S. S. In *Chemical Principles*, 4th ed.; Houghton Mifflin Co: Boston, 2002; pp 457–494.

[31] Payne, M. C.; Teter, M. P.; Allan, D. C.; Arias, T. A.; Joannopoulos, J. D. *Rev. Mod. Phys.* **1992**, *64*, 1045–1097.

[32] Kresse, G.; Furtmüller, J. *Computational Materials Science* **1996**, *6*, 15–50.

[33] Bengtsson, L. *Phys. Rev. B* **1999**, *59*, 12301–12304.

[34] Kozin, I. N.; Deegan, M. J. *A study of the performance of LAPACK symmetric matrix diagonalisers on multi-core architectures*, Daresbury laboratory technical report, Science and Technology Facilities Council, 2007.

[35] Dongarra, J. J.; Croz, J. D.; Hammarling, S.; Duff, I. *ACM Transactions on Mathematical Software* **1990**, *16*, 18–28.

[36] Karlberg, G. S.; Rossmeisl, J.; Nørskov, J. K. *Phys. Chem. Chem. Phys.* **2007**, *9*, 5158–5161.

[37] Gileadi, E.; Kirowa-Eisner, E.; Penciner, J. *Interfacial electrochemistry: An experimental approach*; Addison-Wesley: Reading, 1975.

[38] Rossmeisl, J.; Skúlason, E.; Björketun, M.; Tripkovic, V.; Nørskov, J. K. *Chem. Phys. Lett.*, Accepted (2008).